Scalar field as a time variable during gravitational evolution

Anna Nakonieczna*
Institute of Physics, Maria Curie-Skłodowska University,
Plac Marii Curie-Skłodowskiej 1, 20-031 Lublin, Poland
Institute of Agrophysics, Polish Academy of Sciences, Doświadczalna 4, 20-290 Lublin, Poland

Jerzy Lewandowski†
Faculty of Physics, University of Warsaw, Pasteura 5, 02-093 Warszawa, Poland
(Dated: September 25, 2015)

Using a scalar field as an intrinsic 'clock' while investigating the dynamics of gravitational systems has been successfully pursued in various researches on the border between classical and quantum gravity. The objective of our research was to check explicitly whether the scalar field can serve as a time variable during dynamical evolution of the matter-geometry system, especially in regions of high curvature, which are essential from the perspective of quantum gravity. For this purpose, we analyzed a gravitational collapse of a self-interacting scalar field within the framework of general relativity. The obtained results indicated that the hypersurfaces of constant scalar field are spacelike in dynamical regions nearby the singularities formed during the investigated process. The scalar field values change monotonically in the areas, in which the constancy hypersurfaces are spacelike.

I. INTRODUCTION

Canonical gravity is an approach to general relativity based on an arbitrary slicing of spacetime into spacelike hypersurfaces labeled by a single parameter, which can be interpreted as a time variable. All possible slicings are physically equivalent. The dynamical evolution in such a system is governed by the Hamiltonian, which is also a constraint and a generator of gauge transformations between the spacelike slices. The quantizations of gravity based on its canonical formulation encounter the so-called problem of time. It is related to the fact that there is no clear notion of time in gravitational systems, which could be transferred from the classical to quantum level. The problem reveals itself as crucial in attempts to define the dynamics of a quantized system.

The idea of using matter to quantify time during the course of gravitational evolution was proposed by DeWitt in [1]. In the context of quantum theory of gravity, it was suggested that the matter content of a spacetime can play a role of a 'clock' when investigating the dynamical behavior of geometry. One of the degrees of freedom of the system is interpreted as a dynamical observer. It serves as a reference for the remaining degrees of freedom, whose dynamics is followed with respect to it. Potentially, this concept can be also applied inversely, i.e., the geometry could be used to introduce a physical time when the dynamical evolution of matter is examined.

The notion of internal time is especially important in non-perturbative quantum gravity, which deals with a problem of investigating time evolution without fixed geometry of a background spacetime [2]. A Hamiltonian which describes quantum evolution of a gravitational field with respect to time measured by a 'physical clock' provided by spacelike constancy hypersurfaces of a scalar field was presented in [3]. It was defined through a regularization procedure based on the Ashtekar variables [4, 5] and the loop representation [6, 7] and was shown to be finite and diffeomorphism invariant. Recently, the idea was developed by applying loop quantum gravity tools. The scalar field, which is an intrinsic element of the model, was treated as the time variable for the relational Dirac observables, whose dynamics could be traced with respect to the field [8, 9].

The scalar field was also used to quantify the passage of time during quantum cosmological evolutions. The studies of the inflation epoch of the Universe in the regime of loop quantum gravity was studied with the use of a scalar field with an arbitrary potential [10]. The gauge for the Hamiltonian constraints was chosen so that the scalar field was constant on spacelike hypersurfaces. Treating the scalar field as a time variable allowed writing the Hamiltonian constraints in the form of a time-dependent Schrödinger equation. A similar approach and a massless scalar field is used in the loop quantum cosmology [11, 12].

The Brans-Dicke scalar field, which is non-minimally coupled to geometry, was also examined as a 'clock' in the quantum cosmological context [13]. It was claimed that since the field is a monotonic function of cosmological time, it may serve as an internal time variable. A spatially flat and isotropic cosmological Brans-Dicke model was quantized within the framework of loop quantum cosmology and the effective Hamiltonian was thus obtained.

A homogeneous, massless, minimally coupled scalar field was used to calculate the tunneling decay rate [14] of a simple harmonic universe [15]. It is a cosmological model, which oscillates due to the presence of a negative cosmological constant and a matter component with re-

* aborkow@kft.umcs.lublin.pl
† Jerzy.Lewandowski@fuw.edu.pl

pulsive gravity. An additional field with negligible contribution to the total energy density of the system, which served as a 'clock', was included within it [16, 17]. Its presence was necessary, because the scale factor, which is the only dynamical variable of the model, is not monotonic in an oscillating universe and hence it cannot be treated as a time variable.

The version of the Wheeler-DeWitt equation, which uses the scalar field as a variable common for internal time and a Hamiltonian evolution parameter, and its quantum counterpart for the timelike case were presented in [18]. The former describes the evolution of four-dimensional Lorentz hypersurfaces embedded in a five-dimensional spacetime, along the massless scalar field. The latter has the form of the Schrödinger equation, i.e., it contains the internal time derivative on the right-hand side and presents the evolution with respect to it.

Apart from the scalar field, dust and radiative fluid were also used to provide a matter degree of freedom, which allowed tracing the temporal evolution of a gravitational system. The comoving coordinates of dust particles and the proper time along the dust world lines served as canonical coordinates in the phase space of the dynamical system [19]. The issue of unitarity of the evolution proceeding in the isotropic and homogeneous Brans-Dicke quantum cosmological model, with a time variable defined by the matter fluid, was discussed in [20].

Despite the important achievements in formulating a consistent description of a time evolution of a gravitational system, which were enabled by treating matter as a time variable, a question about the relevance of such an approach remains open. In general, it is assumed that the behavior of matter is desirable during the investigated part of an evolution, i.e., that the spacelike character of the chosen spacetime slices is preserved and that the selected time parametrization remains monotonic during its course. However, the arguments in favor of these assumptions are limited to certain cases (such as homogeneity of a scalar field during an initial phase of inflation, which results in a spacelike character of constant field hypersurfaces [10]) and there does not exist a general justification for them. While for perturbations of the cosmological spatially homogeneous solutions it is plausible that the constancy surfaces of the scalar field are still spacelike, a character of those surfaces is highly non-trivial in the case of the spherically symmetric gravitational collapse. The latter is also a hot subject of quantum gravity [21].

In the present paper we considered an evolution of a scalar field, which was its dynamical gravitational collapse, within the framework of a four-dimensional formulation of general relativity. The main objective of the research was to examine the feasibility of using the scalar field as a time variable in spacetime regions of high curvature, which are essential for the applications of the quantum theory of gravity. The problem was posed and its theoretical formulation was introduced in Section II. Section III contains the description of numerical algorithm used during computations, the specifics of its implementation and its tests. The results were presented and discussed in Section IV, while conclusions were gathered in Section V.

II. THEORETICAL FRAMEWORK

The Lagrangian of the scalar field Φ is

$$\mathcal{L} = \nabla_\alpha \Phi \nabla_\beta \Phi g^{\alpha\beta} \tag{1}$$

and its stress-energy tensor has the form

$$T_{\mu\nu} = \nabla_\mu \Phi \nabla_\nu \Phi - \frac{1}{2} g_{\mu\nu} g^{\alpha\beta} \nabla_\alpha \Phi \nabla_\beta \Phi, \tag{2}$$

where $g_{\mu\nu}$ is a metric tensor of spacetime. The equation of motion for the scalar field derived from the variational principle is

$$\Box \Phi = 0. \tag{3}$$

The gravitational collapse was investigated in spherical symmetry. Since the evolving field is massless, it is convenient to follow the process in double null coordinates $x^\mu = (u, v, \theta, \phi)$, in which the line element has the form

$$ds^2 = -a^2 du dv + r^2 d\Omega^2, \tag{4}$$

where a and r are arbitrary functions of the retarded time u and the advanced time v, while $d\Omega^2 = d\theta^2 + \sin^2\theta d\phi^2$ is the line element of the unit sphere, θ and ϕ are angular coordinates. The employed method is referred to as the 2+2 formalism [22].

The scalar field equation (3) written in the selected coordinates is

$$r\Phi_{,uv} + r_{,u}\Phi_{,v} + r_{,v}\Phi_{,u} = 0 \tag{5}$$

and the Einstein equations for the gravitational field are the following:

$$r r_{,uv} + r_{,u} r_{,v} + \frac{a^2}{4} = 0, \tag{6}$$

$$\frac{a_{,uv}}{a} - \frac{a_{,u} a_{,v}}{a^2} + \frac{r_{,uv}}{r} + \Phi_{,u}\Phi_{,v} = 0, \tag{7}$$

$$r_{,uu} - 2\frac{a_{,u} r_{,u}}{a} + r\Phi_{,u}^2 = 0, \tag{8}$$

$$r_{,vv} - 2\frac{a_{,v} r_{,v}}{a} + r\Phi_{,v}^2 = 0, \tag{9}$$

where $_{,x^\mu}$ denotes the partial derivative.

The system of equations (5) – (9) describes the spherically symmetric dynamical gravitational collapse of a scalar field in double null coordinates. The particulars of the numerical algorithm employed to solve the above equations and its tests are presented in Section III.

The only arbitrary initial data of the computations is the profile of the evolving scalar field, which is imposed on the null $u = const.$ hypersurface. The initial hypersurface will be denoted as $u = 0$ for further convenience.

The investigated families of initial profiles are presented in Fig. 1. They are one-parameter classes of functions parametrized by the amplitude A_Φ. The values of A_Φ used in the plots were chosen so that the collapse resulted in a singular spacetime, as will be explained in more detail below. From now on, the profiles presented in Fig. 1 with the amplitudes specified in its caption will be referred to as profiles P1 to P9. The profiles describe spherically symmetric shells of matter as they tend to zero for $v \to \infty$ and $v \to 0$. The former condition ensures asymptotic flatness of spacetime. The latter is equivalent to vanishing as $r \to 0$, because the gauge freedom of equations in v-coordinate was thus fixed, see Section III.

III. NUMERICAL COMPUTATIONS

The considered dynamical gravitational collapse is described by second-order differential equations (5) – (9). In order to solve the system numerically a set of auxiliary variables was introduced

$$c = \frac{a_{,u}}{a}, \quad d = \frac{a_{,v}}{a}, \quad f = r_{,u}, \quad g = r_{,v}, \quad x = \Phi_{,u}, \quad y = \Phi_{,v}. \tag{10}$$

The quantities f and g are related to the expansions θ_u and θ_v of the null geodesic vector fields ∂_u and, respectively, ∂_v via $\theta_u = 2r^{-1}f$ and $\theta_v = 2r^{-1}g$ [23]. The hypersurfaces determined by $f = 0$ and $g = 0$ are the trapping and anti-trapping horizons in the spacetime, respectively [24]. The squares of the quantities x and y represent fluxes of the scalar field through null hypersurfaces of constant v and u, respectively. The substitutions (10) allowed us to obtain the system of first-order differential equations, which determines the course of the investigated process

$$V1 : a_{,u} - ac = 0, \tag{11}$$
$$V2 : a_{,v} - ad = 0, \tag{12}$$
$$V3 : r_{,u} - f = 0, \tag{13}$$
$$V4 : r_{,v} - g = 0, \tag{14}$$
$$V5 : \Phi_{,u} - x = 0, \tag{15}$$
$$V6 : \Phi_{,v} - y = 0, \tag{16}$$
$$E1 : f_{,u} = 2cf - rx^2, \tag{17}$$
$$E2 : g_{,v} = 2dg - ry^2, \tag{18}$$
$$E3 : f_{,v} = g_{,u} = -\lambda r^{-1}, \tag{19}$$
$$E4 : c_{,v} = d_{,u} = \lambda r^{-2} - xy, \tag{20}$$
$$S : \; rx_{,v} = ry_{,u} = -\eta, \tag{21}$$

where $\lambda = \frac{a^2}{4} + fg$ and $\eta = gx + fy$. The evolution of d and y along u was governed by relations $E4$ and S, respectively. The remaining quantities, that is a, Φ, g, r, f and x, evolved along the v-coordinate according to equations $V2$, $V6$, $E2$, $V4$, $E3$ and S. The function c did not play an active role during the computations, so it was ignored.

The evolution was followed on a two-dimensional grid constructed in the (vu)-plane with integration steps in v and u directions denoted as h_v and h_u, respectively, and initially equal to 10^{-4}. The numerical algorithm proposed in [25] was implemented. The general form of equations (11) – (21) can be written as

$$\mathsf{f}_{,u} = \mathsf{F}\left(\mathsf{f}, \mathsf{g}\right), \qquad \mathsf{g}_{,v} = \mathsf{G}\left(\mathsf{f}, \mathsf{g}\right). \tag{22}$$

Calculating a value of the particular function $\mathsf{f}(u, v)$ or $\mathsf{g}(u, v)$ at the point (v_0, u_0) required the knowledge of the values of functions F and G at points $(v_0 - h_v, u_0)$ and $(v_0, u_0 - h_u)$

$$\mathsf{f}\big|_{(v_0,u_0)} = \frac{1}{2}\Big(\mathsf{ff}\big|_{(v_0,u_0)} + \mathsf{f}\big|_{(v_0,u_0-h_u)} + h_u \mathsf{F}\left(\mathsf{ff}, \mathsf{gg}\right)\big|_{(v_0,u_0)}\Big), \tag{23}$$

$$\mathsf{g}\big|_{(v_0,u_0)} = \frac{1}{2}\Big(\mathsf{gg}\big|_{(v_0,u_0)} + \mathsf{g}\big|_{(v_0-h_v,u_0)} + h_v \mathsf{G}\left(\mathsf{ff}, \mathsf{gg}\right)\big|_{(v_0,u_0)}\Big), \tag{24}$$

where two types of auxiliary quantities were introduced

$$\mathsf{ff}\big|_{(v_0,u_0)} = \mathsf{f}\big|_{(v_0,u_0-h_u)} + h_u \mathsf{F}\left(\mathsf{f}, \mathsf{g}\right)\big|_{(v_0,u_0-h_u)}, \tag{25}$$

$$\mathsf{gg}\big|_{(v_0,u_0)} = \mathsf{g}\big|_{(v_0-h_v,u_0)} + \frac{h_v}{2}\Big(\mathsf{G}\left(\mathsf{f}, \mathsf{g}\right)\big|_{(v_0,u_0)} + \mathsf{G}\left(\mathsf{ff}, \mathsf{gg}\right)\big|_{(v_0,u_0)}\Big). \tag{26}$$

Double null coordinates ensured regular behavior of all the evolving quantities within the domain of integration except the vicinity of $r = 0$. During numerical computations considerable difficulties also arose nearby the event horizon, where the function f was discontinuous. A dense numerical grid was necessary to conduct the calculations in the neighborhood of the event horizon and to examine the behavior of fields beyond it, especially for large values of advanced time. Since regions in which the dense grid was required were well-defined within the domain of integration, an adaptive grid was implemented in order to perform calculations with a smaller step where necessary. An algorithm which enabled us to make the grid denser in the u-direction was implemented, as it was sufficient for the conducted analyses [26]. A local truncation error indicator was the function $\Delta_u r \cdot r^{-1}$, where $\Delta_u r$ is a difference between the values of r for the fixed v at two adjacent hypersurfaces of constant u. It was used to mark areas where the denser mesh was required because it changed its value significantly in adequate regions [27].

Boundary conditions of the process were determined along the line $u = v$. The spacetime containing a spherically symmetric shell of matter is flat inside the shell

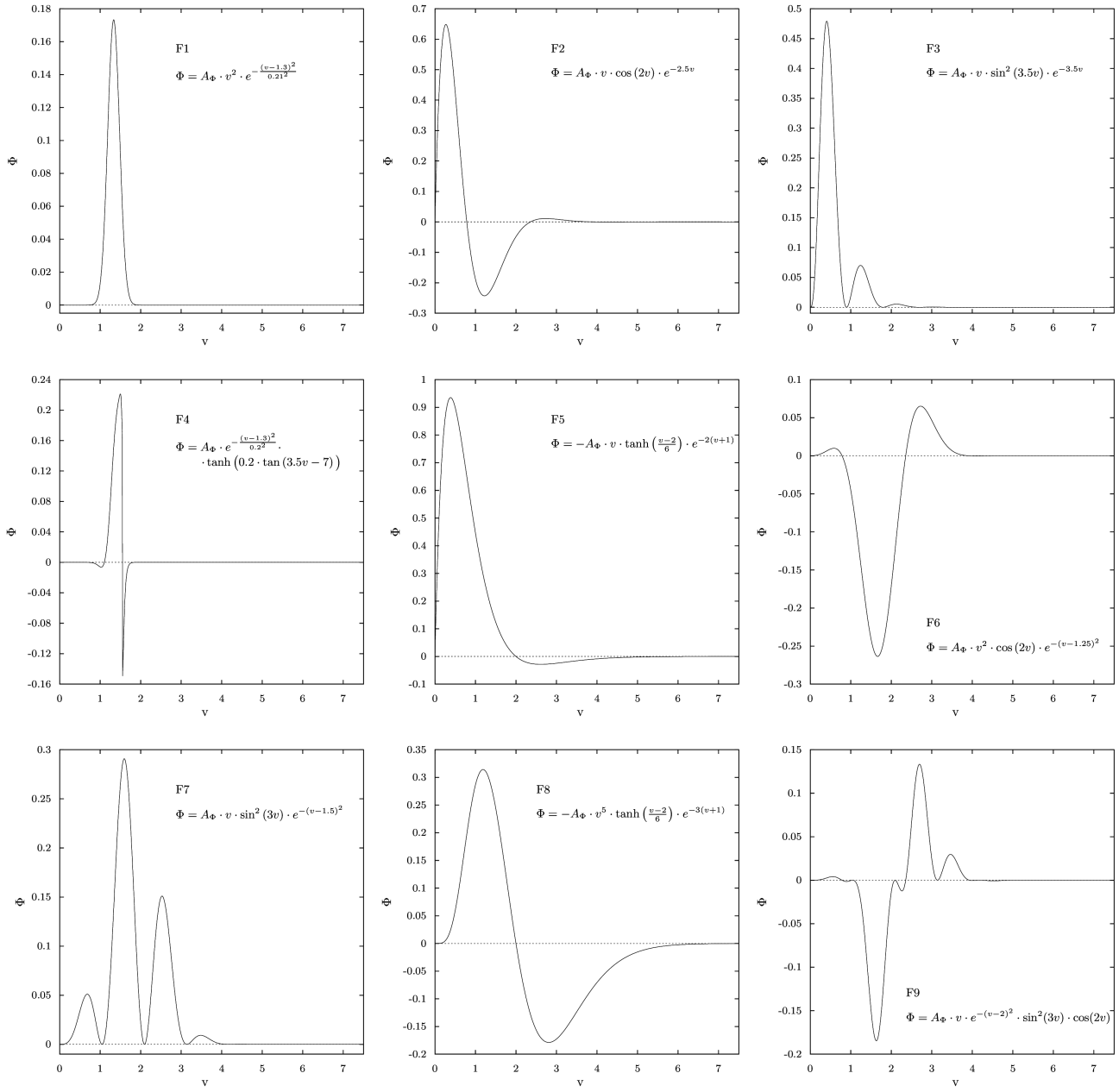

FIG. 1. Families of the scalar field initial profiles $\Phi(0, v)$. The amplitudes A_Φ were set as equal to 0.1, 5.5, 5.0, 0.75, 147.5, 0.115, 0.185, 700 and 0.135 for families F1 to F9, respectively.

and at large radii from it. This fact justified an assumption that the line $u = v$ was not affected by the presence of collapsing matter and its vicinity was nearly flat, which gave $r = 0$ along $u = v$. Using the equation $E3$ the boundary condition $\lambda = 0$ was obtained, which in combination with equations $V3$ and $V4$ led to $f = -g = -\frac{a}{2}$. The requirement $\Phi_{,r} = a_{,r} = 0$ along $u = v$ guaranteed the flattening of the functions nearby $r = 0$, which made the numerical analysis possible. Since r was a nonlinear function of both null coordinates, the three-point regressive derivative method with a variable step was used to implement this boundary condition, apart from the first point where the Euler's method was used. Due to the form of the equation S the relation $\eta = 0$ held along $u = v$. The definition of η gave $x = y$ along this line. Boundary conditions for the quantities evolving along the u-coordinate were obtained according to the equation (23) with auxiliary quantities (26) taken as equal to the corresponding functions at $r = 0$.

Initial conditions were formulated along an arbitrarily chosen null hypersurface, denoted as $u = 0$. The assump-

tion of a negligible spacetime curvature in the area where the collapse begins justified the condition $d(0,v) = 0$, which finally fixed the remaining gauge freedom in v-coordinate. The flatness of spacetime in the vicinity of the line $u = v$, which was discussed above, gave $a(0,v) = 1$. As was mentioned in Section II, the only arbitrary initial condition was the profile of the scalar field $\Phi(0,v)$. The quantity $y(0,v)$ was computed analytically using the equation $V6$. The evolution of functions g, r, f and x was followed using the three-point Simpson's method except the first point, where the Newton's method was implemented.

The accuracy of the program was tested in two ways, namely the convergence of the obtained results and mass conservation in spacetime were checked. In order to monitor the convergence of the code computations for all the examined initial profiles (presented in Fig. 1) were conducted on four grids, whose integration steps were multiples of 10^{-4}. A step of a particular grid was twice the size of a denser one. The convergence was examined on $u = const.$ hypersurfaces chosen for each profile arbitrarily. The values of retarded time were selected so that the hypersurface was situated close to the event horizon, but in the region where the adaptive grid was yet inactive, which was necessary for performing a proper comparison of results.

The field functions along the selected hypersurfaces of constant u are shown in Fig. 2. The areas in which the differences among functions obtained on various grids were most significant were magnified. The maximum discrepancy between the finest and coarsest grids equal to 2.6% was observed for the profile P5. The remaining profiles displayed even better behavior, because the above-mentioned differences did not exceed 1.3%. Figure 3 presents the linear convergence of the numerical code. The maximal divergence between profiles obtained on two grids with a quotient of integration steps equal to 2 and their respective doubles was 3.4%. As expected, the errors became smaller linearly as the grid density increased. The convergence analysis revealed that both the proposed algorithm and the numerical code were adequate for solving the system of equations (11) – (21) with all investigated initial profiles P1 to P9.

The mass conservation in the obtained spacetimes was investigated with the use of a notion of Hawking mass [28]. It is a quasi-local mass function, which for the Schwarzschild-type spacetimes in double null coordinates can be written as [25]

$$m(u,v) = \frac{r}{2}\left(1 + \frac{4r_{,u}r_{,v}}{a^2}\right) = \frac{r}{2}\left(1 + \frac{4}{a^2}fg\right) \quad (27)$$

and it describes the mass included in a sphere of the radius $r(u,v)$. The Hawking mass as a function of retarded time along the line $v = 7.5$, which was a maximal value of advanced time achieved numerically, for all the investigated families of initial profiles is presented in Fig. 4. Since during the evolution the matter was scattered by the gravitational potential barrier when the collapsing

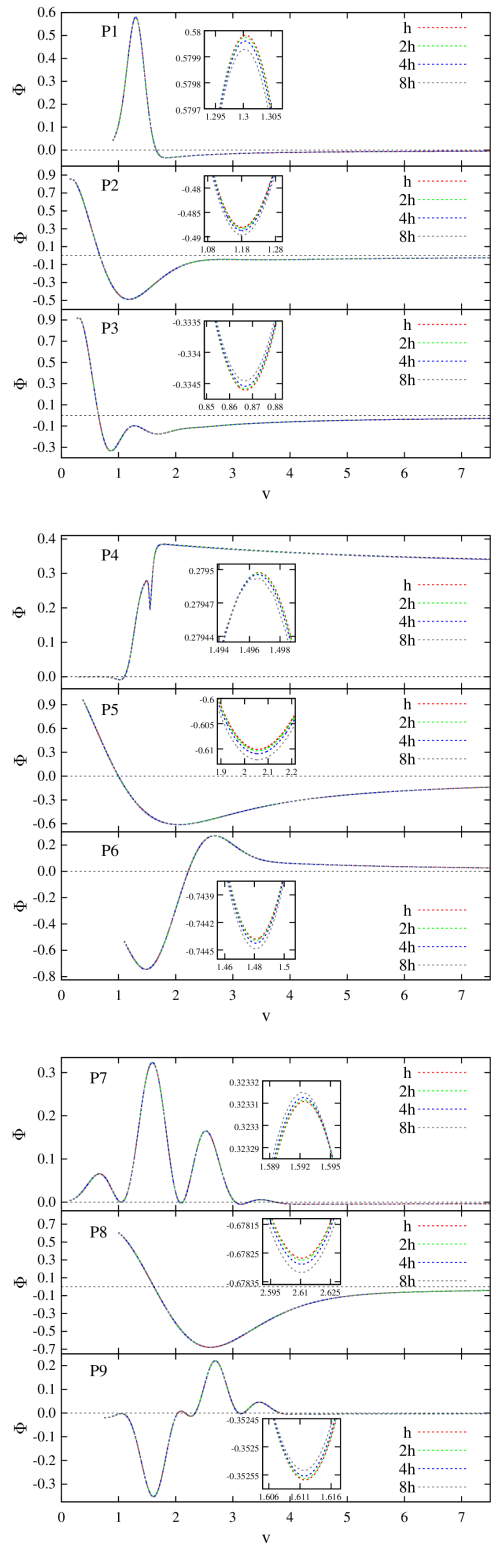

FIG. 2. (Color online) The convergence of the scalar field function during the collapse initiated with the examined profiles. The functions $\Phi(v)$ were plotted for evolutions conducted with integration steps, which were multiples of $h = 10^{-4}$, along hypersurfaces of constant u equal to 0.9, 0.1504, 0.2752, 0.3, 0.3752, 1.1, 0.1504, 1.0 and 0.7504 for profiles P1 to P9, respectively.

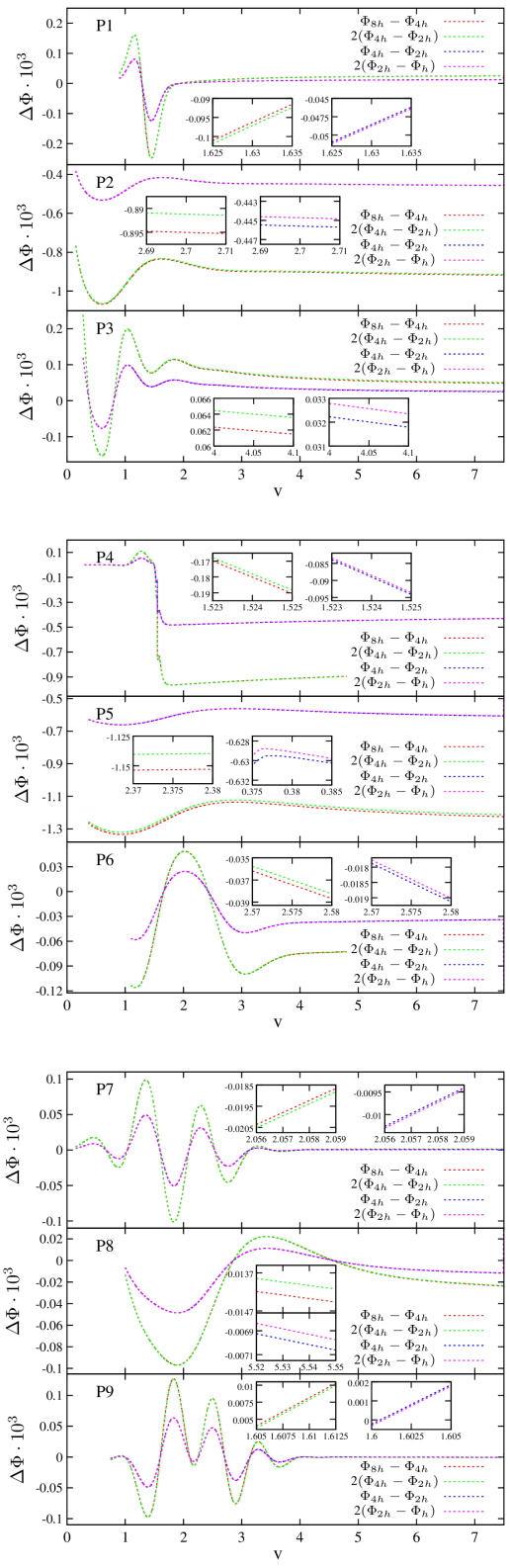

FIG. 3. (Color online) The linear convergence of the code. The differences between field functions calculated on grids with different integration steps (multiples of $h = 10^{-4}$) and their doubles were obtained for profiles P1 to P9 along the same hypersurfaces of constant u as in Fig. 2.

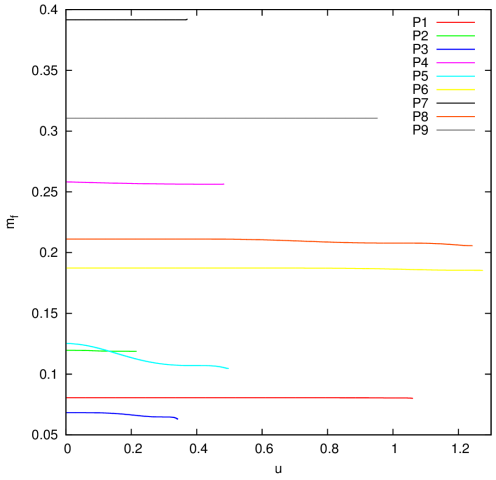

FIG. 4. (Color online) Hawking masses calculated along $v = 7.5$, m_f, as functions of retarded time, u, for spacetimes obtained with initial profiles P1 to P9.

shell approached its gravitational radius, the mass conservation law was not satisfied in the entire domain of integration. The effect of the outgoing mass flux was negligible except the vicinity of the event horizon. The deviation from mass constancy increased with advanced time, as the event horizon was approached. The maximal percentage deviations from mass conservation for the initial profiles P1 to P9 are presented in Table I. In the majority of cases they were smaller than 1.0%. The most significant deviation, exceeding 16%, was observed for the profile P5. Table I also presents the values of u corresponding to the event horizon locations and to the percentage deviations not exceeding 5%. The analysis of mass conservation in spacetime led to the conclusion that the behavior of matter investigated numerically for all initial profiles was correct within the domain of integration. Only the results obtained for the profile P5 should be treated with reserve, but they were also not excluded from further analysis by the performed code accuracy checks.

During the computations the fulfillment of equalities $f_{,v} = g_{,u}$ and $x_{,v} = y_{,u}$, which stem from the substitutions (10), was monitored for all the examined profiles. The checks were performed in both null directions along $v = v_f$ and constant u, whose values for the particular profiles were gathered in the caption of Fig. 2. The necessary derivatives were calculated with the use of the three-point regressive derivative method. The relations $f_{,v} = g_{,u}$ and $x_{,v} = y_{,u}$ were satisfied with an accuracy of 5.8% and 2.5% along the constant u hypersurfaces. The accuracy at $v = const.$ was equal to 2.5% and 0.1%, respectively. The discrepancies increased as $r \to 0$ at $u = const.$ and as $u \to u_{EH}$ at constant v. The obtained accuracies of the constraints confirmed the correctness of the code.

TABLE I. The maximal percentage deviations from mass conservation, DEV, the values of retarded time corresponding to the event horizon location, u_{EH}, and to the percentage deviations from mass conservation not exceeding 5%, u_5, for the investigated initial profiles.

Profile	P1	P2	P3	P4	P5	P6	P7	P8	P9
DEV [%]	0.65	0.7	7.85	0.62	16.27	0.97	0.21	2.53	0.13
u_{EH}	1.0609	0.2154	0.3421	0.4697	0.4954	1.2729	0.2858	1.2367	0.9331
u_5	–	–	0.2631	–	0.1309	–	–	–	–

IV. RESULTS

The dynamical spacetime resulting from the scalar field gravitational collapse is either non-singular or it contains a black hole of a Schwarzschild-type, i.e., a spacelike singularity situated along $r = 0$ surrounded by one horizon. The final outcome of the process depends on the value of the amplitude A_Φ, which determines the strength of a self-interaction of the scalar field. Since we were interested in the behavior of the scalar field in regions of high curvature, i.e., nearby the singularity, we focused on amplitudes leading to the formation of a black hole in spacetime. They were selected for every family of initial profiles separately and their values are given in the caption of Fig. 1.

Penrose diagrams of the obtained dynamical spacetimes, which present $r = const.$ lines in the (vu)-plane with θ and ϕ suppressed, are shown in Fig. 5. The central singularity is situated along the non-linear part of the outermost $r = const.$ line, which was bolded on the diagrams. It is spacelike, because the derivative $\frac{du}{dv}\big|_{r=0}$ is negative along the line. The singularity is surrounded by a single apparent horizon, marked red on the diagrams, which is situated along a hypersurface, which becomes null in the region where $v \to \infty$. As an apparent horizon coincides with an event horizon in static spacetimes, it is postulated that its null character at infinity indicates the location of the event horizon in spacetime. Event horizons of the emerging spacetimes were presented as green dashed null lines on the Penrose diagrams.

The location of an apparent horizon in the particular spacetime allows us to divide the neighborhood of the central singularity into two parts. The first one corresponds to the range of the v-coordinate, within which the apparent horizon changes its position along u. This region will be referred to as dynamical, because the apparent horizon is situated inside the event horizon, which is a characteristic property of dynamical spacetimes [29]. In this area the actual dynamics of the collapse takes place, before the spacetime settles down as $v \to \infty$. The remaining part of the vicinity of the singularity is related to the apparent horizon being situated along a null hypersurface. This region will be dubbed as non-dynamical. The null hypersurfaces of constant v which are borders between the dynamical and non-dynamical regions for spacetimes obtained with the use of profiles P1 to P9 are pictured on the plots in Fig. 5 as blue dashed lines. The respective values of advanced time, v_{dyn}, are presented on the adequate diagrams.

The values of v_{dyn} were calculated on the basis of examining the changes of u and v-coordinates along the apparent horizon. The changes of retarded time (δu) are constant due to the construction of the numerical grid (see Section III). The differences in advanced time (δv) on adjacent $u = const.$ hypersurfaces vary from δu to the values of an order of $10^4 \delta u$. The values of δv close to δu are characteristic for the dynamical region, while the growth of δv means that the apparent horizon settles along $u = const.$ indicating the non-dynamical area. The selected value of v_{dyn} was the biggest value of advanced time corresponding to $\delta v \geqslant 10^2 \delta u$.

The condition which has to be fulfilled in order to treat the dynamical scalar field as a time variable is that the lines of constant values of the field are spacelike. The trajectories of $\Phi = const.$ lines in spacetimes emerging from the collapse initiated with the use of the profiles P1 to P9 are presented in Fig. 6. The spacetime regions, in which the lines are spacelike were marked gray on the plots and the dynamical areas nearby central singularities were magnified. The character of the particular constant Φ line was determined on the basis of the sign of the derivative $\frac{du}{dv}\big|_{\Phi=const.}$ calculated along it. The areas of spacelike and timelike hypersurfaces $\Phi = const.$ were characterized by positive and negative values of the derivatives, respectively.

It may be inferred from the diagram for the profile P1 that in the vicinity of the singularity the lines of constant Φ are spacelike, except for a limited area, in which the lines are timelike or null and which seems to have one boundary point situated at the singularity. The area is situated outside of the dynamical part of the vicinity of the singularity. Hence, nearby the central singularity the scalar field can be treated as a time variable.

The interpretation of the results obtained for the remaining initial profiles is analogous, having in mind two disparities. Firstly, the amount of the above-mentioned areas, whose boundaries have single common points with the singularity, depend on the family of the initial profile and these areas can be situated within the dynamical regions nearby the singularity (e.g., profiles P3, P7 and P9). Secondly, there can exist certain regions situated in non-dynamical parts of the neighborhoods of the singularities, in which the $\Phi = const.$ lines are non-spacelike (e.g., pro-

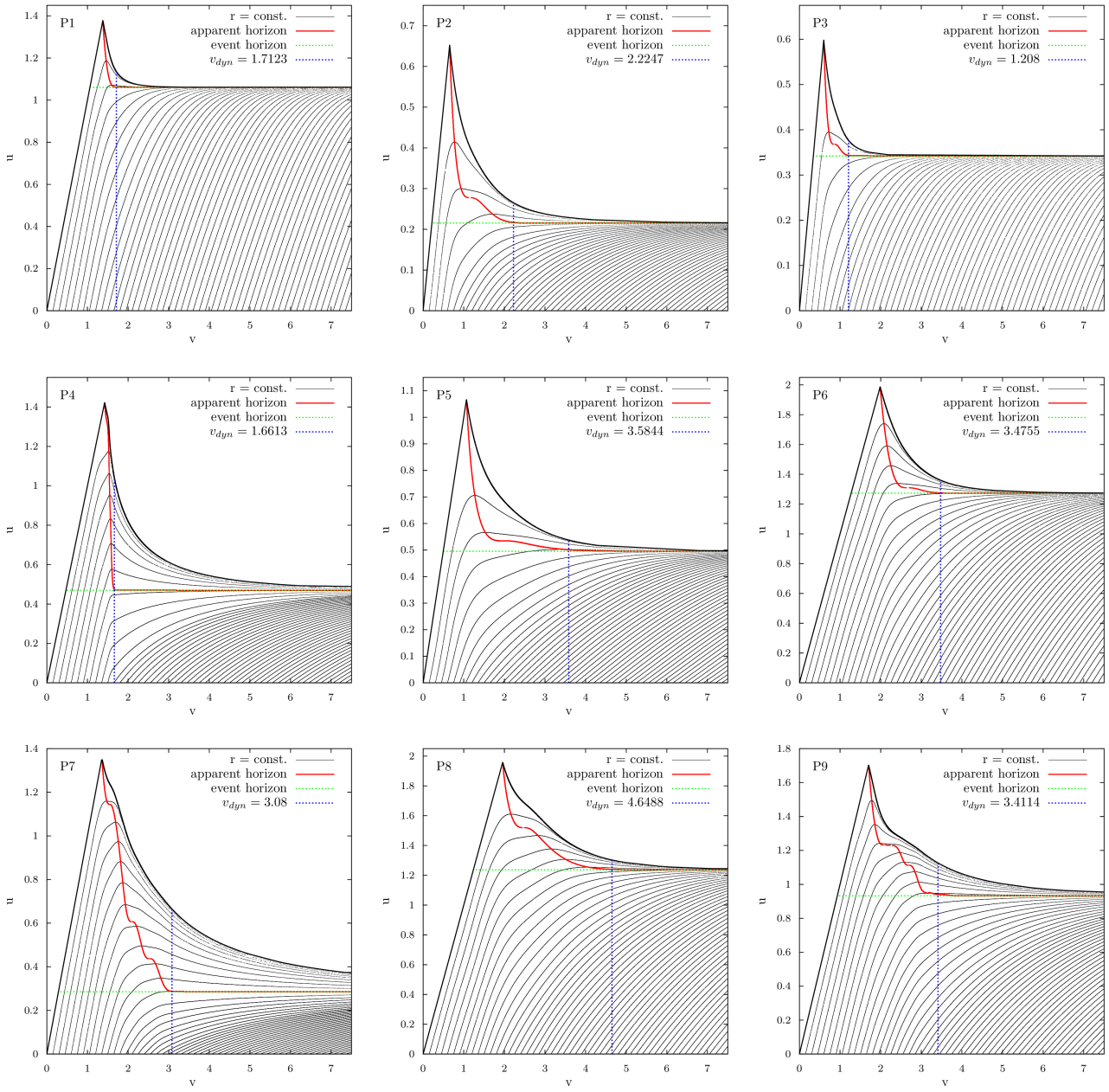

FIG. 5. (Color online) Penrose diagrams of dynamical Schwarzschild spacetimes formed during the scalar field gravitational collapse with initial profiles P1 to P9. The borders between dynamical and non-dynamical regions are situated along null hypersurfaces denoted as v_{dyn}.

files P4, P8 and P9). Despite the outlined differences, the results obtained for all the profiles enhance the comprehensiveness of the conclusion that a scalar field can be treated as a time variable safely, at least in the dynamical part of the vicinity of the singularity of the evolving spacetime.

Another requirement, which is crucial for treating the scalar field as a time variable is its monotonicity in the regions of interest. An inspection of the course of lines of constant Φ shown on the plots in Fig. 6 allows us to draw a conclusion that in the regions, where the lines are spacelike, the changes are monotonic along constant u and v. Since the time coordinate is defined as $t = \frac{u+v}{2}$ in double null coordinates and the t-axis forms an angle of 45° with both u and v axes, the above conclusion can be extended to the coordinate t. The non-monotonic behavior of $\Phi = const.$ lines arises only when areas of spacelike and timelike or null characters are considered, which is excluded regarding the aforementioned demand of the spacelike nature of constancy hypersur-

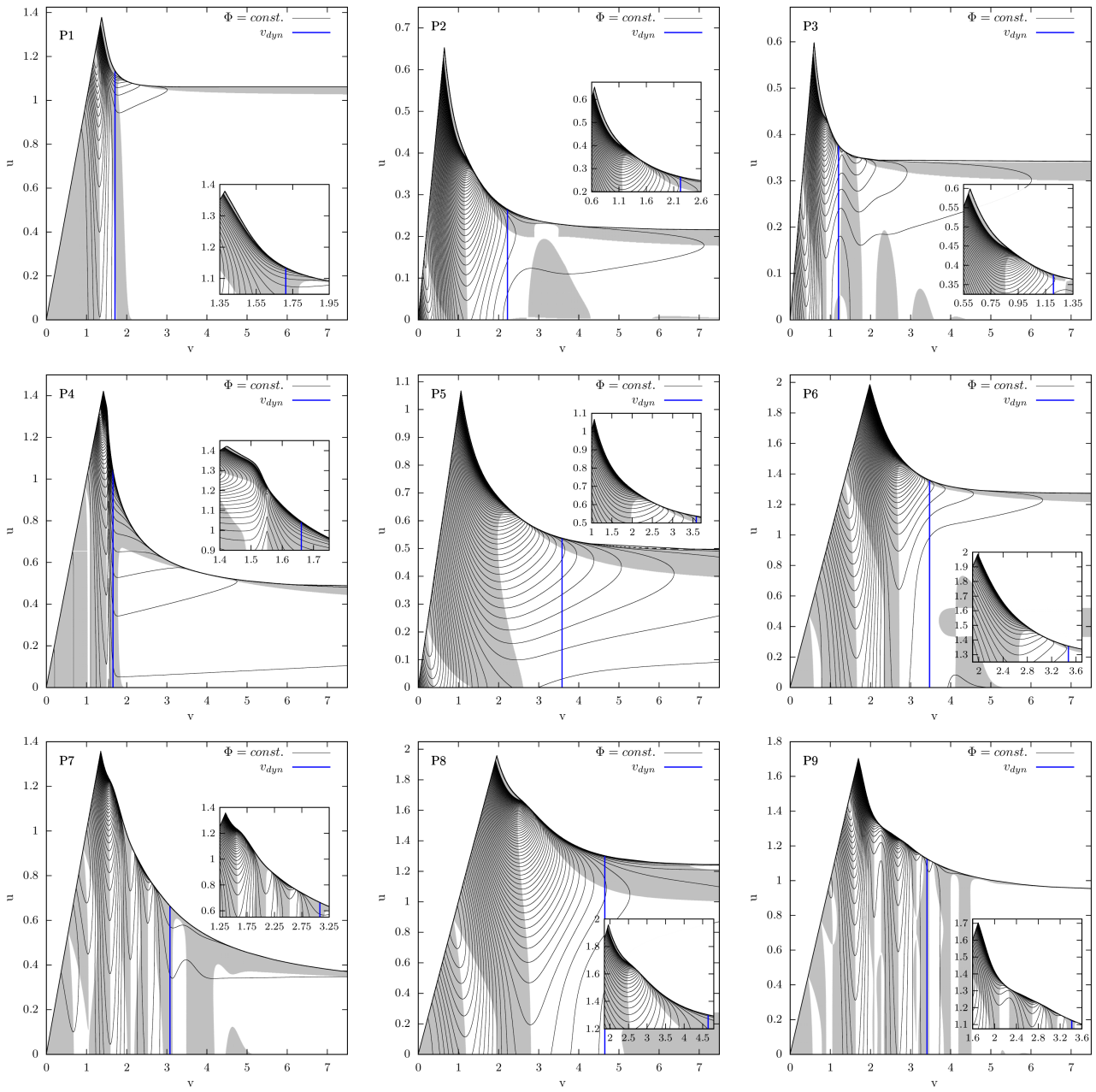

FIG. 6. (Color online) Lines of constant Φ in spacetimes developed during the gravitational collapse of a scalar field with initial profiles P1 to P9. Gray areas indicate spacetime regions, in which the hypersurfaces $\Phi = const.$ are spacelike. The dynamical regions in the vicinities of central singularities were magnified.

faces of Φ.

An important aspect of the conducted analysis, which stems from the fact that the numerical methods were employed, is whether the singularity was approached closely enough in order to draw conclusions about the behavior of the evolving field in its close proximity. The estimation of the singularity closeness which was achieved during numerical computations is presented in Table II. It was made along the whole central singularity on the basis of the relation between the value of the radial function r which refers to the location of the event horizon in spacetime, r_{EH}, and its lowest value obtained in the course of simulations, r_{min}. It turned out that the minimal values of the radial function are at least six orders of magnitude smaller in comparison to the ones which refer to the event horizon location. This defines the relative degree of numerical closeness to the singularity obtained during the evolution of the scalar field.

It should be stressed that the presented analysis is valid for the investigated families of profiles presented in Fig. 1,

TABLE II. Computational closeness to the singularity. r_{EH} denotes the value of the radial function related to the event horizon location in spacetime, while r_{min} is the minimum value of r, which was achieved numerically in the vicinity of the central singularity.

Profile	P1	P2	P3	P4	P5	P6	P7	P8	P9
r_{EH}	0.16003	0.23711	0.12424	0.51198	0.20897	0.36999	0.78311	0.41127	0.62098
$r_{min} \cdot 10^7$	11.23	2.60	1.88	0.48	0.20	18.72	1.74	0.36	52.65
$\frac{r_{min}}{r_{EH}} \cdot 10^7$	70.17	10.97	15.13	0.94	0.93	50.60	2.22	0.88	84.79

which means that it is independent of the selected values of initial amplitudes A_Φ. Due to the widely accepted property of the scalar field dynamical collapse, which is its independence of the type of the initial profile [30], the conclusions can be also extended to other profiles having properties described at the end of Section II.

V. CONCLUSIONS

The possibility of investigating dynamics of quantum gravitational systems with respect to one of their matter components has been successfully exploited in various researches within quantum gravity. In our paper we made an attempt to justify using a scalar field as an intrinsic 'clock' during investigations of dynamical systems. For this purpose, we analyzed a dynamical evolution of a self-interacting scalar field within the framework of general relativity, for a collection of nine different initial configurations of the field.

As a result of each evolution a Schwarzschild spacetime was obtained. It contained a spacelike singularity surrounded by an apparent horizon, which for all investigated initial conditions was spacelike in the dynamical part of the spacetime. This is an interesting observation when associated with the notion of dynamical horizons, which are quasi-local spacelike horizons used to investigate numerous diversified aspects of physics of evolving black holes [31].

The interpretation of the results was concentrated on the issue, whether the evolving scalar field fulfills the necessary requirements to be regarded as a time variable. Our studies led to the following conclusions.

1. The lines of constant scalar field are spacelike in the dynamical part of the vicinity of the central spacelike singularity formed during the dynamical gravitational collapse for all the investigated families of initial profiles. For families F4, F8 and F9 there exist regions situated in non-dynamical areas, in which the lines are timelike or null.

2. The scalar field values change monotonically with u, v and t coordinates in the regions, in which the hypersurfaces of constant Φ are spacelike.

3. The distance from the central singularity achieved numerically was estimated in relation to the location of the event horizon in spacetime. Although numerical computations did not allow us to trace the scalar field evolution precisely up to the central singularity, the relative distance from it was at least six orders of magnitude smaller than the event horizon location, which means that it was highly satisfactory in the context of investigating the behavior of the field in its vicinity.

The above findings revealed that the scalar field can be treated as a time variable in dynamical parts of evolving spacetimes for certain, while the non-dynamical parts should be treated cautiously. It should be stressed that the presented outcomes are valid for the massless scalar field coupled to gravity only. In the case of more complicated gravitational systems, using matter which is coupled not only to gravity, but also to additional matter fields, as a time measurer requires separate investigations, probably adapted to the specific problem. Some indications that matter-geometry systems, which include non-minimally coupled Brans-Dicke field and a real or complex scalar field can admit intrinsic 'clocks' can be found in [32, 33].

ACKNOWLEDGMENTS

This work was partially supported by the Polish National Science Center Grant No. 2011/02/A/ST2/00300.

[1] B. S. DeWitt, Phys. Rev. **160**, 1113 (1967).
[2] C. Rovelli, Phys. Rev. D **43**, 442 (1991).
[3] C. Rovelli and L. Smolin, Phys. Rev. Lett. **72**, 446 (1994).
[4] A. Ashtekar, Phys. Rev. Lett. **57**, 2244 (1986).
[5] A. Ashtekar, Phys. Rev. D **36**, 1587 (1987).
[6] C. Rovelli and L. Smolin, Phys. Rev. Lett. **61**, 1155 (1988).
[7] C. Rovelli and L. Smolin, Nucl. Phys. B **331**, 80 (1990).
[8] M. Domagała, K. Giesel, W. Kamiński, and J. Lewandowski, Phys. Rev. D **82**, 104038 (2010).

[9] J. Lewandowski, M. Domagała, and M. Dziendzikowski, Proc. Sci. QGQGS 2011 , 025 (2012).
[10] S. Alexander, J. Malecki, and L. Smolin, Phys. Rev. D **70**, 044025 (2004).
[11] A. Ashtekar, T. Pawłowski, and P. Singh, Phys. Rev. Lett. **96**, 141301 (2006).
[12] A. Ashtekar, T. Pawłowski, and P. Singh, Phys. Rev. D **74**, 084003 (2006).
[13] X. Zhang, M. Artymowski, and Y. Ma, Phys. Rev. D **87**, 084024 (2013).
[14] M. Dąbrowski and A. L. Larsen, Phys. Rev. D **52**, 3424 (1995).
[15] P. W. Graham, B. Horn, S. Kachru, S. Rajendran, and G. Torroba, JHEP **1402**, 029 (2014).
[16] A. T. Mithani and A. Vilenkin, JCAP **01**, 028 (2012).
[17] A. T. Mithani and A. Vilenkin, Phys. Rev. D **91**, 123511 (2015).
[18] L. Perlov, Phys. Lett. B **743**, 143 (2015).
[19] J. D. Brown and K. V. Kuchar, Phys. Rev. D **51**, 5600 (1995).
[20] C. R. Almeida, A. B. Batista, J. C. Fabris, and P. R. L. V. Moniz, Gravit. Cosmol. **21**, 191 (2015).
[21] R. Gambini and J. Pullin, AIP Conf. Proc. **1647**, 19 (2015).
[22] J. Winicour, Living Rev. Rel. **12**, 3 (2009).
[23] H. Maeda, T. Harada, and B. J. Carr, Phys. Rev. D **79**, 044034 (2009).
[24] S. A. Hayward, Phys. Rev. D **49**, 6467 (1994).
[25] R. S. Hamadé and J. M. Stewart, Class. Quant. Grav. **13**, 497 (1996).
[26] A. Borkowska, M. Rogatko, and R. Moderski, Phys. Rev. D **83**, 084007 (2011).
[27] Y. Oren and T. Piran, Phys. Rev. D **68**, 044013 (2003).
[28] S. W. Hawking, J. Math. Phys. **9**, 598 (1968).
[29] S. W. Hawking and G. F. R. Ellis, *The large scale structure of spacetime* (Cambridge University Press, 1973).
[30] M. W. Choptuik, Phys. Rev. Lett. **70**, 9 (1993).
[31] A. Ashtekar and B. Krishnan, Living Rev. Rel. **7**, 10 (2004).
[32] D. Hwang and D. Yeom, Class. Quant. Grav. **27**, 205002 (2010).
[33] J. Hansen and D. Yeom, JHEP **10**, 040 (2014).